Publication II

Piippo, A. and Luomi, J. (2005). “Adaptive observer combined with HF signal injection for sensorless control of PMSM drives.” In *Proceedings of the IEEE International Electric Machines and Drives Conference (IEMDC’05)*, pp. 674–681, San Antonio, TX.

Adaptive Observer Combined With HF Signal Injection for Sensorless Control of PMSM Drives

Antti Piippo and Jorma Luomi
Power Electronics Laboratory
Helsinki University of Technology
P.O. Box 3000, FI-02015 TKK, Finland

Abstract— **The paper presents a speed and position estimation method for the sensorless control of permanent magnet synchronous motors. The method is based on a speed-adaptive flux observer that is augmented with a high-frequency signal injection technique at low speeds and standstill. In the adaptive observer, a flux model is used as the reference model and a voltage model as the adaptive model. At low speeds, the estimation is further corrected with an error signal from the signal injection method by influencing the direction of the estimated stator flux. The fast dynamic response of the adaptive observer is thus combined with the steady-state accuracy of the high-frequency signal-injection method. According to simulations and experiments, the proposed approach is stable and robust, and can cope with stepwise changes in the speed or position reference. The capability of rejecting load torque transients is also good.**

I. Introduction

Vector control of a permanent magnet synchronous motor (PMSM) requires information of the rotor position. In sensorless control, the rotor speed and position are estimated without mechanical sensors. The estimation methods can be classified into two main strategies: fundamental-excitation methods and signal injection methods.

Fundamental-excitation methods are based on the dynamic model of the motor. The estimation algorithm can be a voltage model or a more complicated observer [1]–[4]. The accuracy of these methods is sufficient at high speeds. Since the back-emf is proportional to the rotor speed, however, problems are encountered at low speeds due to the limited accuracy of measurements and parameter estimates, and due to the presence of inverter nonlinearities.

Signal injection methods are based on detecting the anisotropy caused by the saliency of the rotor or by magnetic saturation. A high-frequency (HF) test signal is superimposed on the stator voltage, and information of the rotor position is obtained from the current response [5]–[7]. If persistent HF excitation is used, the voltage carrier signal either revolves at high angular frequency [6]–[9] or alternates in the estimated rotor reference frame [10]–[14]. The rotor position can be estimated by a synchronous tracking scheme [6], [8], [10]–[13], which means that an error signal is driven to zero by the observer, or the rotor angle (or angle error) can be evaluated directly from the current response [7], [9], [14].

Fundamental-excitation methods have good dynamic properties, but they do not allow sustained operation at low speeds. On the other hand, signal injection methods are well suited to operation at low speeds, including standstill, but tend to have limited dynamic performance. Therefore, a combination of a fundamental-excitation method and an HF signal injection method might be a good solution when a wide speed range, including low-speed operation, is required. An approach for combining the methods was already discussed in [15]. A hybrid scheme combining a fundamental-wave flux observer with an HF signal injection method has been proposed for the rotor flux estimation of induction motors in [16]. For PMSM drives, a fundamental-excitation method is used above a certain speed limit and the estimation method is switched to signal-injection at low speeds and standstill in [17]–[19]. A recently presented method uses a combination of a voltage model and HF signal injection at low speeds [20]. The information included in the fundamental-excitation method improves the dynamic behavior of the rotor position estimation.

This paper proposes coupling the HF signal injection to a more advanced observer. A speed-adaptive observer is used throughout the whole speed range. At low speeds, the estimation is augmented with an HF signal injection method, stabilizing the adaptive observer. The methods are combined by means of correcting the direction of the estimated stator flux. The proposed combination of the two methods results in an observer having good steady-state accuracy and excellent dynamic properties over a wide speed range.

II. PMSM Model

The PMSM is modeled in the d-q reference frame fixed to the rotor. The d axis is oriented along the permanent magnet flux, whose angle in the stator reference frame is θ_m in electrical radians. The stator voltage components are

$$u_d = R_s i_d + \frac{d\psi_d}{dt} - \omega_m \psi_q \tag{1a}$$

$$u_q = R_s i_q + \frac{d\psi_q}{dt} + \omega_m \psi_d \tag{1b}$$

where i_d and i_q are the stator current components, R_s is the stator resistance, and $\omega_m = d\theta_m/dt$ the electrical angular speed of the rotor. The stator flux components are

$$\psi_d = L_d i_d + \psi_{pm} \tag{2a}$$

$$\psi_q = L_q i_q \tag{2b}$$

where L_d and L_q are the d- and q-axis inductances, respectively, and ψ_{pm} is the permanent magnet flux. The electro-

0-7803-8987-5/05/$20.00 ©2005 IEEE.

magnetic torque is given by

$$T_e = \frac{3p}{2}\left[\psi_{pm} i_q + (L_d - L_q) i_d i_q\right] \tag{3}$$

where p is the number of pole pairs.

III. Observer Structure

A. Adaptive Observer

In an adaptive observer, the rotor speed and position estimation is based on the estimation error between two different models (a reference model and an adaptive model) [21]–[23]. The estimated variable can be the stator flux or the stator current, in which case the reference model is the motor itself. An error term is constructed from the two estimates, and used in an adaptation mechanism. The output of the adaptation mechanism, usually the rotor speed or position, is used as a correction in the adaptive model.

In the following, the stator flux is estimated with two models, and the estimate of the rotor speed is used for adjusting the adaptive model. The observer is formulated in the (estimated) rotor reference frame. The reference model is based on (2); this flux model can be written as

$$\hat{\psi}_{d,i} = \hat{L}_d i_d + \hat{\psi}_{pm} \tag{4a}$$

$$\hat{\psi}_{q,i} = \hat{L}_q i_q \tag{4b}$$

where estimated quantities are denoted by $\hat{}$.

The adaptive model is based on (1) and (2). It is here referred to as a voltage model, and defined by

$$\frac{d\hat{\psi}_{d,u}}{dt} = u_d - \hat{R}_s \hat{i}_d + \hat{\omega}_m \hat{\psi}_{q,u} + \lambda \tilde{i}_d \tag{5a}$$

$$\frac{d\hat{\psi}_{q,u}}{dt} = u_q - \hat{R}_s \hat{i}_q - \hat{\omega}_m \hat{\psi}_{d,u} + \lambda \tilde{i}_q \tag{5b}$$

where

$$\hat{i}_d = \frac{\hat{\psi}_{d,u} - \hat{\psi}_{pm}}{\hat{L}_d} \tag{6a}$$

$$\hat{i}_q = \frac{\hat{\psi}_{q,u}}{\hat{L}_q} \tag{6b}$$

are the estimates for the stator current components and

$$\tilde{i}_d = i_d - \hat{i}_d \tag{7a}$$

$$\tilde{i}_q = i_q - \hat{i}_q \tag{7b}$$

are the components of the current error. λ is a gain parameter, which can be selected as $\lambda \geq -\hat{R}_s$. By selecting $\lambda = -\hat{R}_s$, (5) becomes a pure voltage model.

There are various alternatives for obtaining an error term from the flux estimates (5) and (4). In the following, the error term is defined

$$F_\varepsilon = \hat{\psi}_{q,i} - \hat{\psi}_{q,u} \tag{8}$$

The estimate of the electrical angular speed of the rotor, used for adaptation in (5), is obtained by a PI-type speed adaptation mechanism

$$\hat{\omega}_m = -k_p F_\varepsilon - k_i \int F_\varepsilon dt \tag{9}$$

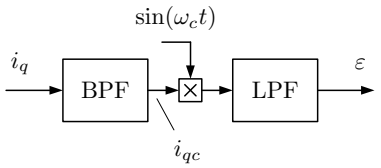

Fig. 1. Principle of the error signal demodulator.

where k_i and k_p are nonnegative gains. The estimate $\hat{\theta}_m$ for the rotor position is obtained by integrating $\hat{\omega}_m$.

B. High-Frequency Signal Injection

An alternating voltage [10] was selected for HF signal injection. A carrier excitation signal fluctuating at angular frequency ω_c and having amplitude $\hat{u}_c$, i.e.,

$$u_c = \hat{u}_c \cos(\omega_c t) \tag{10}$$

is superimposed on the d component of the stator voltage in the estimated rotor reference frame. An alternating HF current response is detected in the q direction of the estimated rotor reference frame, amplitude modulated by the rotor position estimation error. The principle of the demodulation scheme is shown in Fig. 1. The q component of the measured current is band-pass filtered (BPF), giving an HF current signal i_{qc} that varies at the signal injection frequency. The current signal is then demodulated and low-pass filtered (LPF) to extract an error signal

$$\varepsilon = \mathrm{LPF}\big\{ i_{qc} \sin(\omega_c t) \big\} \tag{11}$$

Ideally, this error signal is [10]

$$\varepsilon = \underbrace{\frac{\hat{u}_c}{\omega_c} \frac{L_q - L_d}{4 L_q L_d}}_{K_\varepsilon} \sin(2\tilde{\theta}_m) \tag{12}$$

where K_ε is the signal injection gain and $\tilde{\theta}_m = \theta_m - \hat{\theta}_m$ is the estimation error of the rotor position.

The demodulation scheme is implemented as follows. The band-pass filtering of i_q is achieved by zero averaging over one period of the carrier signal, i.e.

$$i_{qc} = i_q - \frac{1}{T_c} \int_{t-T_c}^{t} i_q dt \tag{13}$$

where $T_c = 2\pi/\omega_c$. The algorithm (13) can be interpreted as a high-pass filter, and its computational cost is lower than that of relevant band-pass filters. The low-pass filtering of the signal $i_{qc} \sin(\omega_c t)$ is implemented using a moving-average filter and a first-order low-pass filter. The moving-average filter removes the angular frequency ω_c and its multiples effectively and causes only a short time delay, while the first-order low-pass filter reduces stochastic noise more effectively than the moving-average filter. After filtering, the amplitude of ε is limited to avoid errors caused by transients in i_q.

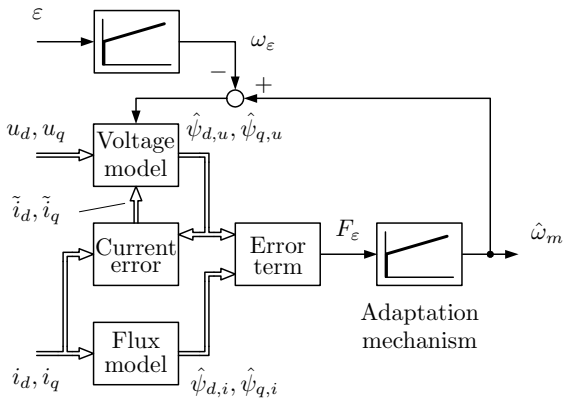

Fig. 2. Block diagram of the combined observer: adaptive observer is augmented with error signal ε from HF signal injection.

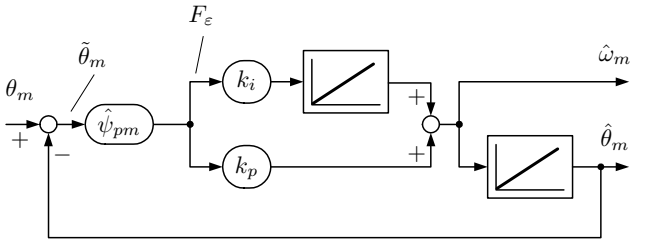

Fig. 3. Block diagram of the phase-locked loop corresponding to the adaptive observer.

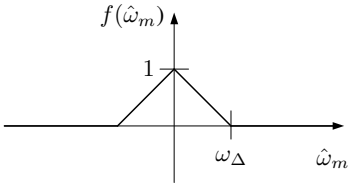

Fig. 4. Definition of the speed-dependent function $f(\hat{\omega}_m)$.

C. Combined Observer

At low speeds, the orientation error of the adaptive observer may become too large for stable operation due to inaccuracies in measurements and parameter estimates. The method proposed in this paper uses the HF signal injection to correct the orientation by influencing the direction of the stator flux estimate.

Fig. 2 shows the block diagram of the adaptive observer enhanced with the HF signal injection. The idea is to use the error signal ε of the signal injection method to adjust the adaptive model (5). A correction ω_ε is subtracted from the speed estimate $\hat{\omega}_m$, and a PI mechanism is used for driving the error signal ε to zero. The algorithm is given by

$$\frac{d\hat{\psi}_{d,u}}{dt} = u_d - \hat{R}_s\hat{i}_d + (\hat{\omega}_m - \omega_\varepsilon)\hat{\psi}_{q,u} + \lambda\tilde{i}_d \tag{14a}$$

$$\frac{d\hat{\psi}_{q,u}}{dt} = u_q - \hat{R}_s\hat{i}_q - (\hat{\omega}_m - \omega_\varepsilon)\hat{\psi}_{d,u} + \lambda\tilde{i}_q \tag{14b}$$

and

$$\omega_\varepsilon = \gamma_p\varepsilon + \gamma_i\int \varepsilon dt \tag{15}$$

where γ_p and γ_i are the gains of the PI mechanism.

At low speeds, the combined observer relies both on the signal injection method and on the adaptive observer: the signal injection method dominates in steady state whereas the adaptive observer commands at transients. When the rotor speed increases above a certain value, the estimation is based only on the adaptive observer.

D. Observer Gain Selection

For selecting the gains k_p and k_i of the adaptation mechanism (9), the observer is interpreted as a phase-locked loop, and the gains are selected according to [11]. The closed-loop system corresponding to the adaptive observer is shown in Fig. 3, where the gain $F_\varepsilon/\tilde{\theta}_m$ is considered approximately equal to the estimated magnitude of the permanent magnet flux. The gains of the adaptation law

$$k_p = \frac{2\alpha_{fo}}{\hat{\psi}_{pm}} \tag{16a}$$

$$k_i = \frac{\alpha_{fo}^2}{\hat{\psi}_{pm}} \tag{16b}$$

are selected using only one design parameter α_{fo}, corresponding to the approximate bandwidth of the adaptive observer.

The PI mechanism (15) can be tuned similarly. The output ω_ε affects indirectly the speed estimate through the estimation of the stator flux in (14). The dynamics of the adaptive observer is assumed much faster than that of the HF signal injection and the PI mechanism and, consequently, the adaptive observer is omitted in the analysis. However, the dynamics of the low-pass filter in (11) are taken into account. In a fashion similar to [20], the bandwidth of the low-pass filter in (11) is selected as

$$\alpha_{lp} = 3\alpha_i \tag{17}$$

and the gains of the PI mechanism are selected as

$$\gamma_p = \frac{\alpha_i}{2K_\varepsilon}, \quad \gamma_i = \frac{\alpha_i^2}{6K_\varepsilon} \tag{18}$$

The parameter α_i is the only required design parameter, corresponding to the approximate bandwidth of the PI mechanism.

In order to obtain a smooth transition between the low-speed and high-speed regions, the amplitude of the signal injection voltage $\hat{u}_c$ and the bandwidth α_i are decreased linearly with increasing speed, and the signal injection is disabled above transition speed ω_Δ, i.e.

$$\hat{u}_c = f(\hat{\omega}_m)\hat{u}_{c0}, \quad \alpha_i = f(\hat{\omega}_m)\alpha_{i0} \tag{19}$$

where $\hat{u}_{c0}$ and α_{i0} are the values corresponding to zero-speed operation and function $f(\hat{\omega}_m)$ is shown graphically in Fig. 4. The parameters α_{lp} and γ_i are varied according to (17), (18), and (12). The parameter γ_p remains constant according to (18) and (12).

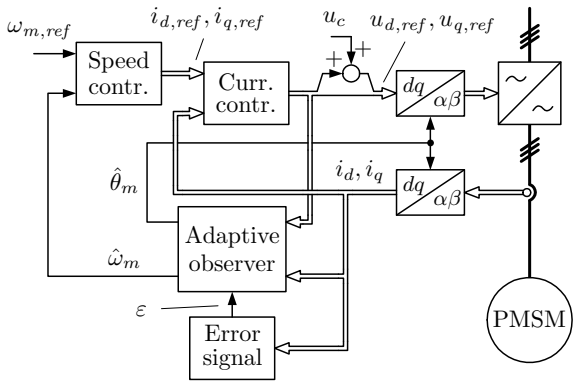

Fig. 5. Block diagram of the control system. Blocks "Error signal" and "Adaptive observer" are shown in Figs. 1 and 2, respectively. Block "Speed contr." includes both the speed controller and the minimization of the current amplitude.

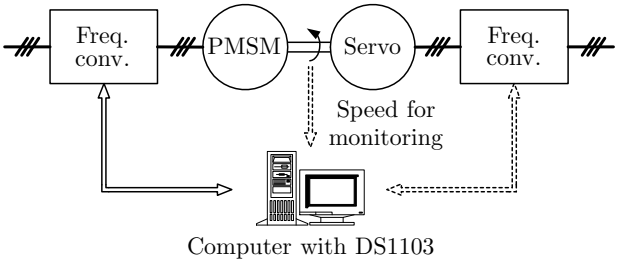

Fig. 6. Experimental setup. Mechanical load is provided by a servo drive.

As the speed increases close to the transition speed ω_Δ, the error signal ε may differ from zero in the steady state, causing integration drift in (15). Therefore, the integral should be bounded within reasonable limits, e.g.,

$$\left|\gamma_i \int \varepsilon dt\right| \leq f(\hat{\omega}_m)\omega_\Delta \tag{20}$$

IV. Control System

The block diagram of the control system comprising cascaded speed and current control loops is shown in Fig. 5. The current control is implemented as PI-type control in the estimated rotor reference frame, where the cross-coupling terms and the back-emf are decoupled [24]. The current is predicted one sampling period ahead [25], [26]. Due to parameter errors, a steady-state error may be present in the predicted current. Hence, the predicted current is not used in the integral part of the current controller.

PI-type speed control with active damping is used. The references $i_{d,ref}$ and $i_{q,ref}$ of the stator current components are calculated according to maximum torque per current control [27]. For position control, a P-type controller is added as the outermost control loop in the control system. The dc-link voltage of the converter is measured, and a simple current feedforward compensation for dead times and power device voltage drops is applied [28].

V. Results

The proposed observer was investigated by means of simulations and laboratory experiments. The experimental setup is illustrated in Fig. 6. A six-pole interior-magnet PMSM (2.2 kW, 1500 rpm) is fed by a frequency converter that is controlled by a dSpace DS1103 PPC/DSP board. Mechanical load is provided by a PMSM servo. An incremental encoder is used only for monitoring the actual rotor speed and position.

TABLE I
Motor Parameters

Nominal power	2.2 kW
Nominal voltage U_N	370 V
Nominal current I_N	4.3 A
Nominal frequency f_N	75 Hz
Nominal speed	1 500 r/min
Nominal torque T_N	14.0 Nm
Number of pole pairs p	3
Stator resistance R_s	3.59 Ω
Direct axis inductance L_d	0.036 H
Quadrature axis inductance L_q	0.051 H
Permanent magnet flux ψ_{pm}	0.545 Vs
Total moment of inertia	0.015 kgm^2

TABLE II
Control System Parameters

Signal-injection angular frequency ω_c	2π1000 rad/s
Signal-injection voltage amplitude $\hat{u}_{c0}$	50 V
Bandwidth of the adaptive observer α_{fo}	2π50 rad/s
Observer gain λ	$-0.2\hat{R}_s$
Bandwidth α_{i0}	2π5 rad/s
Transition speed ω_Δ	2π10 rad/s
Current controller bandwidth	2π400 rad/s
Speed controller bandwidth	2π5 rad/s
Position controller bandwidth	2π1.33 rad/s

The motor parameters are given in Table I and the parameters of the control system in Table II. The base values of voltage, current and angular frequency are $\sqrt{2}U_N$, $\sqrt{2}I_N$, and $2\pi f_N$, respectively. The dc-link voltage is 540 V, and the switching frequency and the sampling frequency are both 5 kHz. The carrier excitation signal has a frequency of 1 kHz and an amplitude of 50 V, and the transition speed $\omega_\Delta = 0.13$ p.u. The electromagnetic torque is limited to 22 Nm, which is 1.57 times the nominal torque.

The MATLAB/Simulink environment was used for the simulations. The parameters listed in Table I were used in the motor model. To illustrate the influence of an error in the stator resistance estimate in the following examples, the estimate was 10 % smaller than the actual stator resistance in the motor model. Moreover, white noise having an rms value of 10 mA was added to the measured phase currents of the motor, and the current signals were quantized in steps of 10 mA.

Fig. 7 shows simulation and experimental results at no load when the speed reference was changed stepwise from zero to 0.2 p.u. at t = 1 s, then reversed to -0.2 p.u. at t = 2 s, and finally set to zero at t = 3 s. The estimated rotor speed follows the actual speed smoothly, and the estimation error $\tilde{\theta}_m$ of the rotor position stays reasonably small, not exceeding 10 electrical degrees.

Fig. 8 depicts simulation and experimental results when the speed reference was set to zero. The load torque was first changed stepwise from zero to the nominal value at

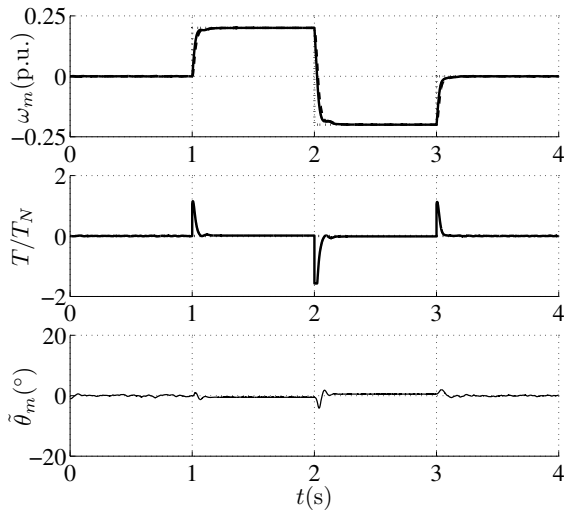

(a)

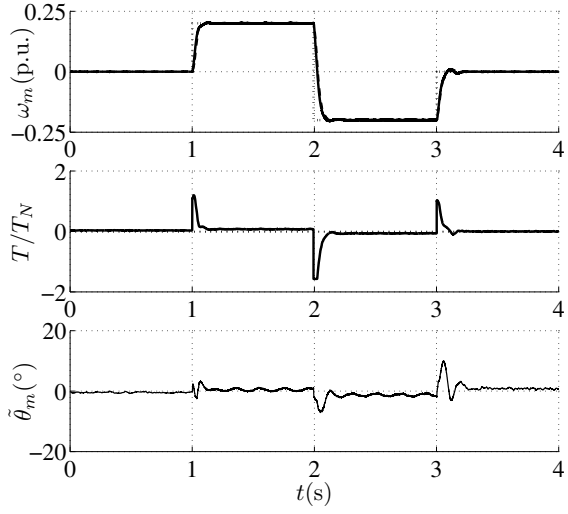

(b)

Fig. 7. Speed reference steps at zero load torque: (a) simulation results; (b) experimental results. First subplot shows electrical angular speed (solid), its estimate (dashed), and its reference (dotted). Second subplot shows estimated electromagnetic torque (solid) and load torque reference (dotted). Last subplot shows estimation error of rotor position in electrical degrees.

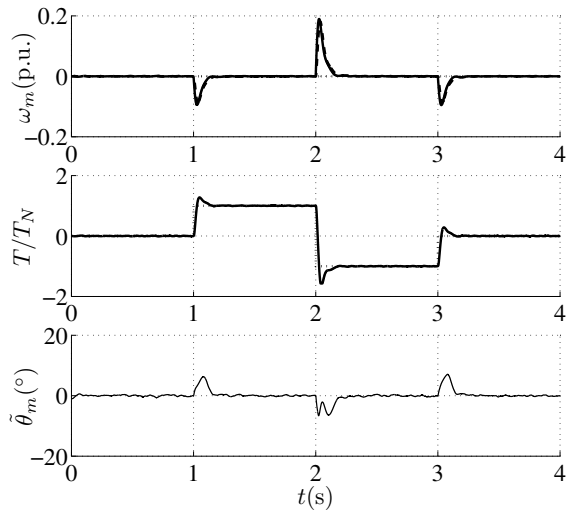

(a)

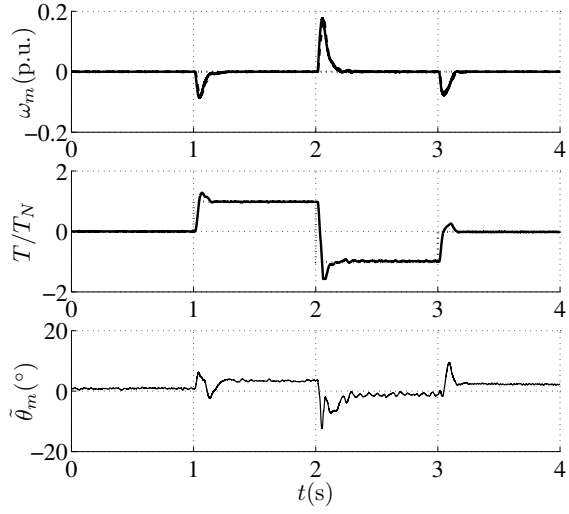

(b)

Fig. 8. Nominal load torque steps at zero speed reference: (a) simulation results; (b) experimental results. Explanations of the curves are as in Fig. 7.

t = 1 s, then reversed at t = 2 s, and removed at t = 3 s. The error of the rotor position estimate is small even during transients, which shows good capability of rejecting fast load torque disturbances. Furthermore, the proposed method allows sustained zero-speed operation at nominal load.

Results at the nominal load torque are shown in Fig. 9. The speed reference was first changed stepwise from zero to 0.33 p.u. at t = 1 s, then reversed to -0.33 p.u. at t = 2 s, and finally set to zero at t = 3 s. The estimated rotor speed follows the actual speed rapidly even during fast changes in the electromagnetic torque.

Results during a slow speed reversal are shown in Fig. 10. The load torque was kept at the nominal value between t = 2 s and t = 28 s, and the speed reference was changed from 0.2 p.u. to -0.2 p.u. between t = 4 s and t = 26 s. The estimated rotor speed follows the actual speed smoothly even during the transitions between the adaptive observer and the combination of the adaptive observer and HF signal injection. At low speeds, some ripple can be seen in measurement results. This ripple is related to the HF signal injection, which is sensitive to inverter nonlinearities and errors in measured phase currents.

Fig. 11 shows simulation and experimental results for the position control at the nominal load torque. The position reference was changed stepwise from zero to one revolution (6π electrical radians) at t = 1 s, then two revolutions backwards at t = 2 s, and finally set to zero at t = 3 s. The position estimate follows the actual value smoothly, and the position settles quickly to its reference value.

In Fig. 12, the position reference was set to zero, while the load torque was first changed stepwise from zero to the nominal value at t = 1 s, then reversed at t = 2 s, and

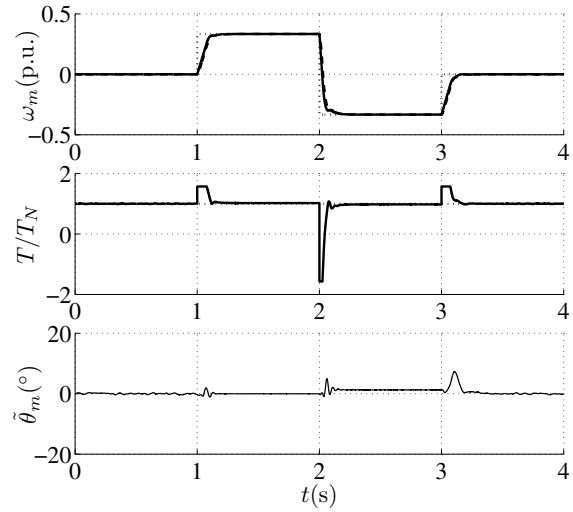

(a)

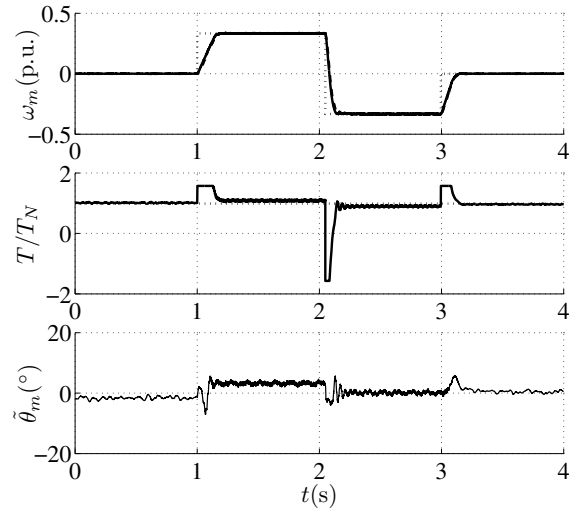

(b)

Fig. 9. Speed reference steps at nominal load torque: (a) simulation results; (b) experimental results. Explanations of the curves are as in Fig. 7.

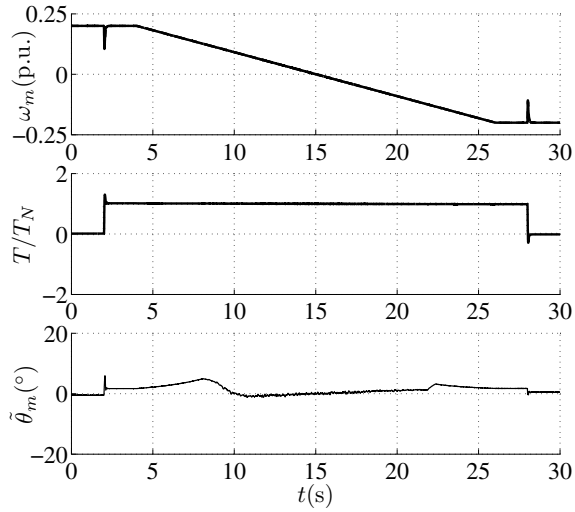

(a)

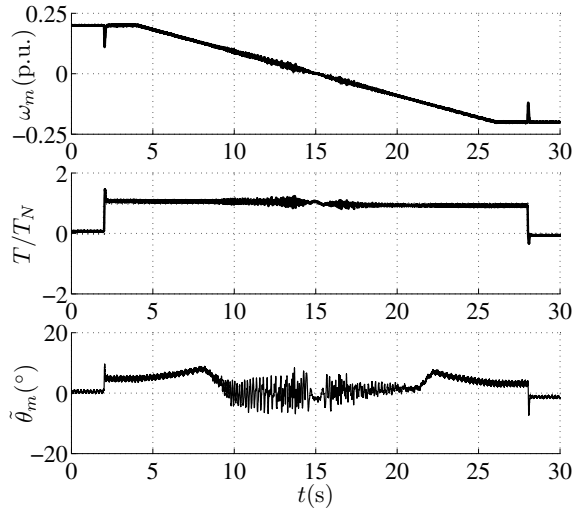

(b)

Fig. 10. Slow speed reversal at nominal load torque: (a) simulation results; (b) experimental results. Explanations of the curves are as in Fig. 7.

removed at t = 3 s. The load torque transients are also rejected effectively in the position control mode.

VI. Conclusions

The rotor speed and position of a permanent magnet synchronous motor can be estimated in a wide speed range, including zero speed, by means of an adaptive observer that is augmented with a high-frequency signal injection technique at low speeds. The fast dynamic response of the adaptive observer is combined with the steady-state accuracy of the high-frequency signal-injection method. According to the simulation and experimental results presented in this paper, the system based on the combined observer is stable and robust, and can cope with stepwise changes in the speed or position reference. The capability of rejecting load torque transients is also good.

Acknowledgment

The authors gratefully acknowledge the financial support given by ABB Oy.

References

[1] R. Wu and G. R. Slemon, "A permanent magnet motor drive without a shaft sensor," *IEEE Trans. Ind. Applicat.*, vol. 27, no. 5, pp. 1005–1011, Sept./Oct. 1991.

[2] R. B. Sepe and J. H. Lang, "Real-time observer-based (adaptive) control of a permanent-magnet synchronous motor without mechanical sensors," *IEEE Trans. Ind. Applicat.*, vol. 28, no. 6, pp. 1345–1352, Nov./Dec 1992.

[3] J. Solsona, M. I. Valla, and C. Muravchik, "A nonlinear reduced order observer for permanent magnet synchronous motors," *IEEE Trans. Ind. Electron.*, vol. 43, no. 4, pp. 492–497, Aug. 1996.

[4] S. Bolognani, R. Oboe, and M. Zigliotto, "Sensorless full-digital PMSM drive with EKF estimation of speed and rotor position," *IEEE Trans. Ind. Electron.*, vol. 46, no. 1, pp. 184–191, Feb. 1999.

[5] M. Schroedl, "Sensorless control of AC machines at low speed and standstill based on the INFORM method," in *Conf. Rec. IEEE-IAS Annu. Meeting*, vol. 1, San Diego, CA, Oct. 1996, pp. 270–277.

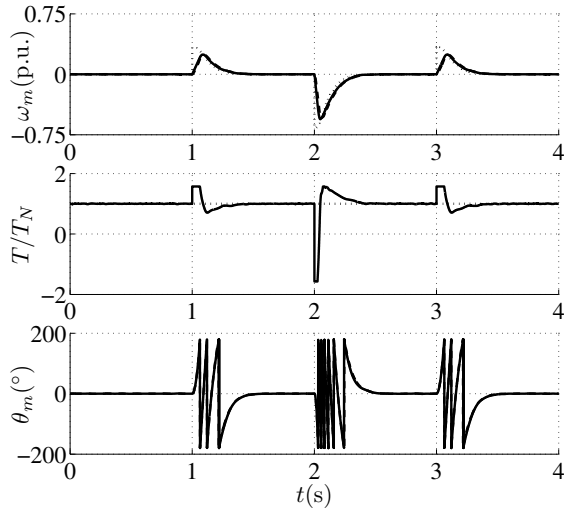

(a)

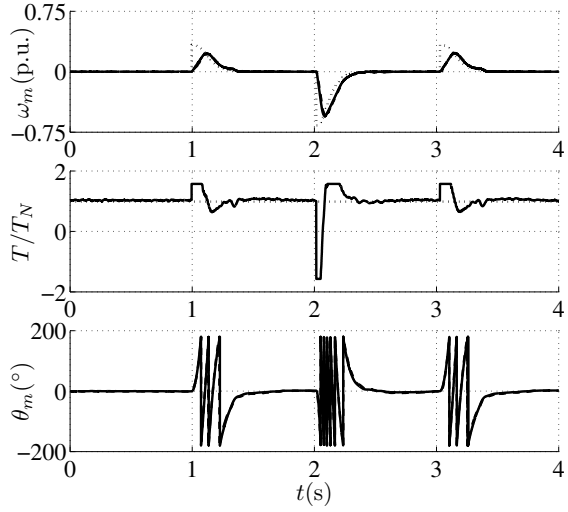

(b)

Fig. 11. Position reference steps at nominal load torque: (a) simulation results; (b) experimental results. First subplot shows electrical angular speed (solid), its estimate (dashed), and its reference (dotted). Second subplot shows estimated electromagnetic torque (solid) and load torque reference (dotted). Last subplot shows rotor position (solid) and its estimate (dashed) in electrical degrees.

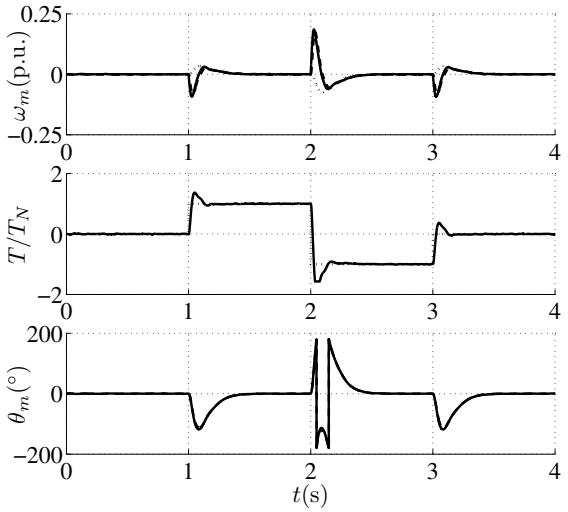

(a)

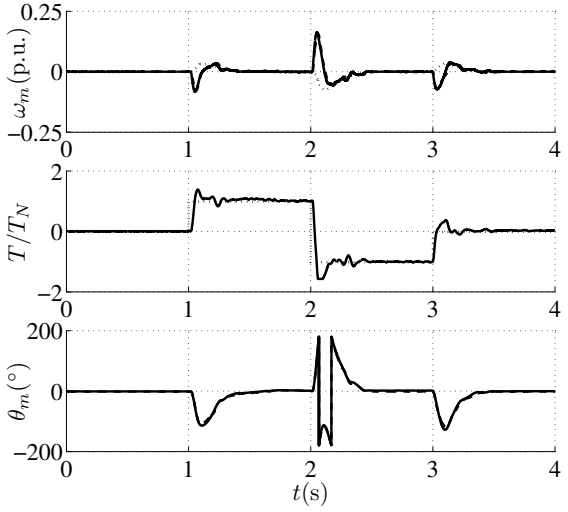

(b)

Fig. 12. Nominal load torque steps at zero position reference: (a) simulation results; (b) experimental results. Explanations of the curves are as in Fig. 11.

[6] P. L. Jansen and R. D. Lorenz, "Transducerless position and velocity estimation in induction and salient AC machines," *IEEE Trans. Ind. Applicat.*, vol. 31, no. 2, pp. 240–247, March/April 1995.

[7] A. Consoli, G. Scarcella, and A. Testa, "Industry application of zero-speed sensorless control techniques for PM synchronous motors," *IEEE Trans. Ind. Applicat.*, vol. 37, no. 2, pp. 513–521, March/April 2001.

[8] L. Wang and R. D. Lorenz, "Rotor position estimation for permanent magnet synchronous motor using saliency-tracking self-sensing method," in *Conf. Rec. IEEE-IAS Annu. Meeting*, vol. 1, Rome, Italy, Oct. 2000, pp. 445–450.

[9] C. Silva, G. M. Asher, M. Sumner, and K. J. Bradley, "Sensorless rotor position control in a surface mounted PM machine using HF rotating injection," *EPE Journal*, vol. 13, no. 3, pp. 12–18, Aug. 2003.

[10] M. Corley and R. D. Lorenz, "Rotor position and velocity estimation for a salient-pole permanent magnet synchronous machine at standstill and high speeds," *IEEE Trans. Ind. Applicat.*, vol. 43, no. 4, pp. 784–789, July/Aug. 1998.

[11] L. Harnefors and H.-P. Nee, "A general algorithm for speed and position estimation of AC motors," *IEEE Trans. Ind. Electron.*, vol. 47, no. 1, pp. 77–83, Feb. 2000.

[12] M. Linke, R. Kennel, and J. Holtz, "Sensorless position control of permanent magnet synchronous machines without limitation at zero speed," in *Proc. IEEE IECON'02*, vol. 1, Sevilla, Spain, Nov. 2002, pp. 674–679.

[13] J. H. Jang, S. K. Sul, J. I. Ha, K. Ide, and M. Sawamura, "Sensorless drive of SMPM motor by high frequency signal injection," in *Proc. IEEE APEC'02*, vol. 1, Dallas, TX, March 2002, pp. 279–285.

[14] F. Parasiliti, R. Petrella, and M. Tursini, "Sensorless speed control of salient rotor PM synchronous motor based on high frequency signal injection and kalman filter," in *Proc. IEEE ISIE'02*, vol. 2, L'Aquila, Italy, July 2002, pp. 623–628.

[15] P. L. Jansen, M. J. Corley, and R. D. Lorenz, "Flux, position, and velocity estimation in ac machines at zero and low speed via tracking of high frequency saliencies," in *Proc. EPE'95*, vol. 3, Sevilla, Spain, Sept. 1995, pp. 154–159.

[16] K. Ide, J.-I. Ha, M. Sawamura, H. Iura, and Y. Yamamoto, "A novel hybrid speed estimator of flux observer for induction motor drives," in *Proc. IEEE ISIE'02*, vol. 3, L'Aquila, Italy, July 2002, pp. 822–827.

[17] E. Robeischl, M. Schroedl, and M. Krammer, "Position-sensorless biaxial position control with industrial PM motor drives based on INFORM-

and back EMF model," in *Proc. IEEE IECON'02*, vol. 1, Sevilla, Spain, Nov. 2002, pp. 668–673.

[18] C. Silva, G. M. Asher, and M. Sumner, "An hf signal-injection based observer for wide speed range sensorless PM motor drives including zero speed," in *Proc. EPE'03*, vol. 1, Toulouse, France, Sept. 2003, pp. 1–9.

[19] M. Tursini, R. Petrella, and F. Parasiliti, "Sensorless control of an IPM synchronous motor for city-scooter applications," in *Conf. Rec. IEEE-IAS Annu. Meeting*, vol. 3, Salt Lake City, UT, Oct. 2003, pp. 1472–1479.

[20] A. Piippo, M. Hinkkanen, and J. Luomi, "Sensorless control of PMSM drives using a combination of voltage model and HF signal injection," in *Conf. Rec. IEEE-IAS Annu. Meeting*, vol. 2, Seattle, WA, Oct. 2004, pp. 964–970.

[21] H. Kubota, K. Matsuse, and T. Nakano, "DSP-based speed adaptive flux observer of induction motor," *IEEE Trans. Ind. Applicat.*, vol. 29, no. 2, pp. 344–348, March/April 1993.

[22] G. D. Andreescu, "Position and speed sensorless control of PMSM drives based on adaptive observer," in *Proc. EPE'99*, Lausanne, Switzerland, Sept. 1999, CD-ROM.

[23] M. Eskola and H. Tuusa, "Sensorless control of a permanent magnet synchronous motor -application to a hoist drive," in *Proc. IEEE PESC'02*, vol. 2, Cairns, Australia, June 2002, pp. 967–972.

[24] F. Briz del Blanco, M. W. Degner, and R. D. Lorenz, "Dynamic analysis of current regulators for AC motors using complex vectors," *IEEE Trans. Ind. Applicat.*, vol. 35, no. 6, pp. 1424–1432, Nov./Dec. 1999.

[25] J. Böcker, J. Janning, and K. Anbuhl, "Realization of a high-dynamic discrete-time controller for PWM inverter-fed induction motor drives," in *Proc. EPE'93*, vol. 4, Brighton, UK, Sept. 1993, pp. 158–162.

[26] L. Springob and J. Holtz, "High-bandwidth current control for torque-ripple compensation in PM synchronous machines," *IEEE Trans. Ind. Electron.*, vol. 45, no. 5, pp. 713–721, Oct. 1998.

[27] T. Jahns, G. Kliman, and T. Neumann, "Interior permanent-magnet synchronous motors for adjustable-speed drives," *IEEE Trans. Ind. Applicat.*, vol. 22, no. 4, pp. 738–747, July/Aug. 1986.

[28] J. K. Pedersen, F. Blaabjerg, J. W. Jensen, and P. Thogersen, "An ideal PWM-VSI inverter with feedforward and feedback compensation," in *Proc. EPE'93*, vol. 5, Brighton, UK, Sept. 1993, pp. 501–507.